

Cite this: *RSC Advances*, 2012, 2, 9130–9134

www.rsc.org/advances

PAPER

Sr₈MgGd(PO₄)₇:Eu²⁺: yellow-emitting phosphor for application in near-ultraviolet-emitting diode based white-light LEDs†

Chien-Hao Huang,^{*ab} De-Yin Wang,^b Yi-Chen Chiu,^a Yao-Tsung Yeh^a and Teng-Ming Chen^{*b}

Received 10th April 2012, Accepted 19th July 2012

DOI: 10.1039/c2ra20646c

The yellow-emitting phosphor Sr₈MgGd(PO₄)₇:xEu²⁺ (SMGP:xEu²⁺) was successfully synthesized by a solid-state reaction and used for the first time to fabricate white light-emitting diodes (LEDs) with excellent color rendering index (CRI). Furthermore, the luminescence properties, reflectance spectra and fabricated LEDs were firstly investigated. The excitation and reflectance spectra of this phosphor show broad band excitation and absorption in the 240–470 nm near ultraviolet (NUV) region, indicating its potential application in NUV diode based white-light LEDs. Upon excitation at 385 nm, the Eu²⁺ doped SMGP phosphors showed strong yellow emission centered at 512 and 606 nm, which could be ascribed to the 4f⁶5d¹ → 4f⁷ transitions of Eu²⁺. The optimal doping concentration of Eu²⁺ in SMGP was determined to be 0.01 mol. Non-radiative transitions between the Eu²⁺ ions in the SMGP host were demonstrated to be attributable to dipole–dipole interactions. A white-light NUV LED was fabricated using a phosphor blend of SMGP:0.01Eu²⁺ and BAM:Eu²⁺ pumped by a 385 nm NUV chip, driven by a 350 mA current. The color, chromaticity coordinates (*x*, *y*), correlated color temperature (CCT) and Commission Internationale de l'Éclairage (CIE) coordinates can be tuned from yellow ((0.442, 0.481), 3456 K, 75.4) through warm white-light ((0.350, 0.348), 4804 K, 95.6) and eventually to white-light ((0.331, 0.321), 5592 K, 94.1) by weight ratio tuning of the SMGP:0.01Eu²⁺ and BAM:Eu²⁺ phosphors, and the luminous efficacy between 9.6 to 7.6 lm W⁻¹. We are currently evaluating the potential applications of SMGP:xEu²⁺ as a yellow-emitting near-ultraviolet (NUV) convertible phosphor in fabricating warm white-light LEDs with excellent CRI.

Introduction

White light-emitting diodes (LEDs) are considered as a promising technology for next generation solid-state lighting systems because they are environmentally friendly and have several advantages such as long operation lifetime, low energy consumption, and high material stability.^{1–4} Typically, white-light LED lamps are fabricated using (a) a combination of trichromatic red-, green-, and blue-emitting LED chips;⁵ (b) blue LED chips combined with a yellow-emitting phosphor (cerium(III) doped yttrium aluminium garnet (YAG:Ce³⁺));⁶ or (c) a blend of red-, green-, and blue-emitting phosphors pumped by ultraviolet (UV; 360–380 nm)/near-ultraviolet (NUV; 380–420 nm) chips.^{7,8} The disadvantages of the combination of trichromatic RGB LEDs system, are that individual colored LEDs respond

differently to drive current, operating temperature, dimming, operating time and the controls needed for color consistency add expense. On the other hand, combining YAG:Ce³⁺ with a blue InGaN chip results in a low color rendering index (CRI) of 75 and a high correlated color temperature (CCT) of 7756 K,⁹ which can be attributed to the lack of red spectral contribution; consequently, the widespread use of such LED systems is severely restricted. In addition, white-light LEDs can be easily fabricated by integrating red, green, and blue phosphors into a UV/NUV chip, but the disadvantages in this case are the high fabrication cost involved and the poor luminous efficiency resulting from energy reabsorption.

During the past few years, white-light LEDs fabricated using NUV chips with a blend of trichromatic red-, green- and blue-emitting phosphors or a combination of yellow- and blue-emitting phosphors have elicited interest, since the CCT and CRI of these LEDs are much greater than those of conventional white-light LEDs. This is because the CCT, CIE chromaticity coordinates, and CRI values of these NUV chip based LEDs can be tuned by changing the R/G/B or Y/B ratio. Hence, the development of new phosphors that can be effectively excited in the NUV range is a very important prospect that requires prompt attention. Several NUV excitable materials have been

^aMaterial and Chemical Research Laboratories, ITRI, Hsinchu, Taiwan, 30011, R.O.C.. E-mail: Chien-Hao@itri.org.tw; Fax: +886-3-5732361; Tel: +886-3-5732438

^bPhosphors Research Laboratory and Department of Applied Chemistry, National Chiao Tung University, Hsinchu, Taiwan, 30010, R.O.C.. E-mail: tmchen@mail.nctu.edu.tw; Fax: +886-3-5723764; Tel: +886-3-5731695

† CCDC 876058. For crystallographic data in CIF format see DOI: 10.1039/c2ra20646c

identified and investigated for use as the host, for example, $\text{Na}_2\text{CaPO}_4\text{F}:\text{Eu}^{2+}$,¹⁰ $\text{Ba}_2\text{Ca}(\text{BO}_3)_2:\text{Ce}^{3+},\text{Mn}^{2+}$,¹¹ $(\text{Sr},\text{Ca})_2\text{P}_2\text{O}_7:\text{Eu}^{2+},\text{Mn}^{2+}$,¹² $\text{Ca}_2\text{PO}_4\text{Cl}:\text{Eu}^{2+}$,¹³ $(\text{Ca},\text{Mg},\text{Sr})_9\text{Y}(\text{PO}_4)_7:\text{Eu}^{2+},\text{Mn}^{2+}$,¹⁴ $\text{Ba}_2\text{ZnS}_3:\text{Mn}^{2+}$,¹⁵ $\text{Ca}_3\text{Si}_2\text{O}_4\text{N}_2:\text{Eu}^{2+}$,¹⁶ $\alpha\text{-Ca}_2\text{P}_2\text{O}_7:\text{Eu}^{2+},\text{Mn}^{2+}$,¹⁷ and $\text{Ca}_3\text{Y}(\text{GaO})_3(\text{BO}_3)_4:\text{Ce}^{3+},\text{Mn}^{2+},\text{Tb}^{3+}$.¹⁸ To the best of our knowledge, however, the crystal structure and luminescence properties of Eu^{2+} activated $\text{Sr}_8\text{MgGd}(\text{PO}_4)_7$ have not yet been reported. In this paper, we report the luminescence properties of the yellow-emitting $\text{Sr}_8\text{MgGd}(\text{PO}_4)_7:x\text{Eu}^{2+}$ phosphor and discuss its application in solid-state lighting. $\text{Sr}_8\text{MgGd}(\text{PO}_4)_7:x\text{Eu}^{2+}$ is shown to be a suitable phosphor for NUV chip excited warm white-light LEDs.

Experimental

Materials and synthesis

Polycrystalline phosphors with the composition $(\text{Sr}_{1-x}\text{Eu}_x)_8\text{MgGd}(\text{PO}_4)_7$ ($\text{SMGP}:x\text{Eu}^{2+}$) are prepared by a high-temperature solid-state reaction. Briefly, the constituent raw materials SrCO_3 (A. R., 99.9%), MgO (A. R., 99%), Gd_2O_3 (A. R., 99.99%), $(\text{NH}_4)_2\text{HPO}_4$ (Merck, $\geq 99\%$), and Eu_2O_3 (A. R., 99.99%) are weighed in stoichiometric proportions and then sintered for 8 h in a reducing atmosphere at 1200 °C. The products are subsequently cooled to room temperature in the furnace, ground, and pulverized for further measurements.

Materials characterization

The crystal structures of the as-synthesized samples were identified by using powder X-ray diffraction (XRD) analysis with a Bruker AXS D8 advanced automatic diffractometer with $\text{Cu-K}\alpha$ radiation ($\lambda = 1.5418 \text{ \AA}$), over the angular range $10^\circ \leq 2\theta \leq 80^\circ$, operating at 40 kV and 40 mA. The photoluminescence (PL) and photoluminescence excitation (PLE) spectra of the samples were analyzed by using a Spex Fluorolog-3 spectrofluorometer equipped with a 450 W Xe light source. The diffuse reflectance (DR) spectra were measured with a Hitachi 3010 double-beam UV-vis spectrometer (Hitachi Co., Tokyo, Japan). The Commission International de l'Eclairage (CIE) chromaticity

coordinates for all samples were measured with a Laiko DT-101 color analyzer equipped with a CCD detector (Laiko Co., Tokyo, Japan).

Results and discussion

Crystal structure

Phase identification for the SMGP and $\text{SMGP}:0.05\text{Eu}^{2+}$ samples was carried out by measuring the XRD profiles, as shown in Fig. 1. The obtained XRD patterns were consistent with those reported in ICSD file no. 59722.¹⁹ XRD analysis was used to determine the chemical purity and phase homogeneity of the SMGP and $\text{SMGP}:0.05\text{Eu}^{2+}$ phosphors. The ionic radius of Eu^{2+} ($r = 1.25 \text{ \AA}$, coordination number (CN) = 8; $r = 1.3 \text{ \AA}$, CN = 9) is the closest to that of Sr^{2+} ($r = 1.26 \text{ \AA}$, CN = 8; $r = 1.31 \text{ \AA}$, CN = 9). Therefore, on the basis of the effective ionic radii and charge balance of cations with different CNs, we proposed that Eu^{2+} should randomly occupy the five Sr^{2+} sites in the SMGP host structure. The lattice parameters of SMGP and $\text{SMGP}:0.05\text{Eu}^{2+}$ (shown in Table 1) were calculated from the experimental XRD profiles using cell refinement software. The lattice parameters of the SMGP powder were as follows: $a = 18.0641(34) \text{ \AA}$, $b = 10.6830(22) \text{ \AA}$, $c = 18.3754(27) \text{ \AA}$, $\beta = 132.930(14)^\circ$, and $V = 2596.4(6) \text{ \AA}^3$. Substitution of Sr^{2+} ions by the relatively smaller Eu^{2+} ions in the SMGP crystal lattice host was confirmed by the decrease in the lattice parameters of $\text{SMGP}:0.05\text{Eu}^{2+}$: $a = 18.0476(44) \text{ \AA}$, $b = 10.6626(27) \text{ \AA}$, $c = 18.3594(17) \text{ \AA}$, $\beta = 132.780(17)^\circ$, and $V = 2593.1(8) \text{ \AA}^3$. These results indicated that Eu^{2+} ions were doped into and entered the SMGP crystal lattice.

Photoluminescence properties

The concentration dependence of the relative PL/PLE intensity of $\text{SMGP}:x\text{Eu}^{2+}$ ($x = 0.005\text{--}0.05 \text{ mol}$) is demonstrated in Fig. 2. The emission spectra showed a strong broad yellow emission band in the range 450–800 nm, centered at 512 and 606 nm, typically attributed to the $4f^65d^1 \rightarrow 4f^7$ electronic dipole allowed transitions of Eu^{2+} ions. The broad asymmetric emission band for $\text{SMGP}:\text{Eu}^{2+}$ was attributed to the transition of Eu^{2+} occupying the five crystallographically distinct Sr^{2+} sites in the SMGP host. The excitation spectra showed a broad band excitation over the range 300–500 nm, centered at 326 and 369 nm; this excitation band mainly comprised unresolved bands due to the $4f^65d^1$ multiplets of Eu^{2+} in the excited state. The optimal Eu^{2+} concentration (x) in $\text{SMGP}:x\text{Eu}^{2+}$ was decided to be 0.01 mol, since further increase in the concentration resulted in concentration quenching, which in turn caused a decrease in the emission intensity. According to the percolation model,^{20,21} concentration quenching can occur by (1) interactions between

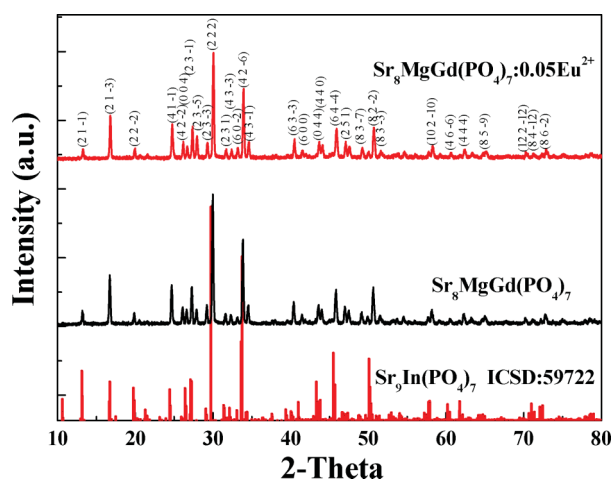


Fig. 1 Powder XRD patterns of $\text{Sr}_8\text{MgGd}(\text{PO}_4)_7$ and $\text{Sr}_8\text{MgGd}(\text{PO}_4)_7:0.05\text{Eu}^{2+}$. The $\text{Sr}_9\text{In}(\text{PO}_4)_7$ standard pattern (ICSD:59722) is shown for reference.

Table 1 Rietveld refinement and crystal data of $\text{Sr}_8\text{MgGd}(\text{PO}_4)_7$ and $\text{Sr}_8\text{MgGd}(\text{PO}_4)_7:0.05\text{Eu}^{2+}$ phosphors

Formula	$\text{Sr}_8\text{MgGd}(\text{PO}_4)_7$	$(\text{Sr}_{0.95}\text{Eu}_{0.05})_8\text{MgGd}(\text{PO}_4)_7$
Formula weight	1547.418	1573.15
$a/\text{\AA}$	18.0641(34)	18.0476(44)
$b/\text{\AA}$	10.6830(22)	10.6626(27)
$c/\text{\AA}$	18.3754(27)	18.3594(34)
$\beta/^\circ$	132.930(14)	132.780(17)
Volume/ \AA^3	2596.4(6)	2593.1(8)

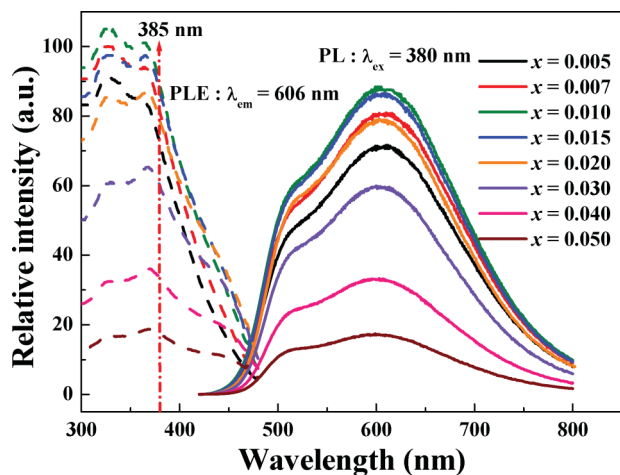


Fig. 2 Concentration dependence of the relative PL/PLE intensity of $\text{Sr}_8\text{MgGd}(\text{PO}_4)_7:\text{xEu}^{2+}$ ($x = 0.005\text{--}0.05$ mol).

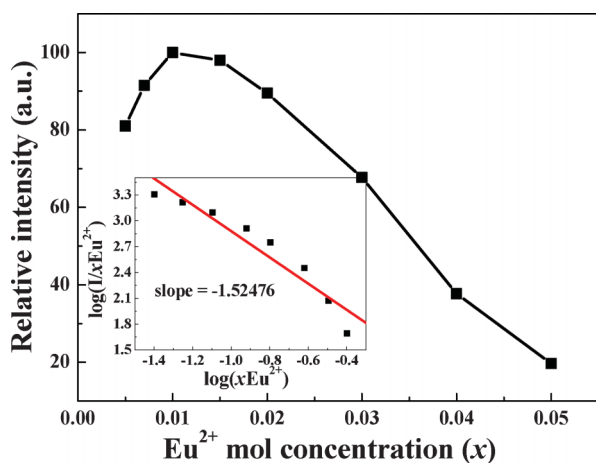


Fig. 3 PL intensity of $\text{Sr}_8\text{MgGd}(\text{PO}_4)_7:\text{xEu}^{2+}$ as a function of Eu^{2+} content under 385 nm excitation. The inset shows the relationship between $\log(x\text{Eu}^{2+})$ and $\log(I/x\text{Eu}^{2+})$.

the Eu^{2+} ions, which result in energy reabsorption among neighboring Eu^{2+} ions in the rare earth sublattice; or (2) energy transfer from a percolating cluster of Eu^{2+} ions to killer centers. With an increase in the Eu^{2+} doping concentration, the excitation edge showed a red shift owing to the enhanced $\text{Eu}^{2+}\text{--Eu}^{2+}$ interactions.

Fig. 3 shows the PL intensity of $\text{SMGP}:\text{xEu}^{2+}$ as a function of Eu^{2+} content ($x = 0.005\text{--}0.05$) under 385 nm excitation. The optimal doping concentration was $x = 0.01$ mol. However, according to the Dexter theory,²² non-radiative transitions between Eu^{2+} ions occur *via* electric multipolar interactions. The mechanism of the interaction between Eu^{2+} ions can be expressed by the following equation:²³

$$\frac{I}{x} = \frac{k}{1 + \beta(x)^{\theta/3}} \quad (1)$$

where χ is the activator concentration; k and β are constants for each interaction for a given host lattice; θ values of 6, 8, and 10 correspond to dipole–dipole, dipole–quadrupole, and quadrupole–quadrupole interactions, respectively.

The relationship between $\log(x\text{Eu}^{2+})$ and $\log(I/x\text{Eu}^{2+})$ is shown in the inset of Fig. 3. The slope of the straight line is $-\theta/3$, and the value of θ is approximately 6. The result indicates that non-radiative transitions between Eu^{2+} ions occur *via* dipole–dipole interactions and lead to concentration quenching of the Eu^{2+} ions in the $\text{SMGP}:\text{xEu}^{2+}$ host, as has been reported previously by our group.²⁴

Reflectance spectra properties

Fig. 4 illustrates the reflectance spectra of SMGP and $\text{SMGP}:0.01\text{Eu}^{2+}$ and the PL/PLE spectra of the $\text{SMGP}:0.01\text{Eu}^{2+}$ phosphor. The reflectance spectrum of the SMGP host showed an absorption band from 240 nm to 400 nm, which was due to the host absorption,²⁵ and the band gap was estimated to be about 4.14 eV. Upon Eu^{2+} doping into the SMGP host, a strong broad band absorption assigned to the $4f^7 \rightarrow 4f^65d^1$ of the Eu^{2+} ions appeared in the wavelength range 240–470 nm (the NUV to blue range). The emission spectra showed a strong broad yellow emission band from 450 to 800 nm, centered at 512 and 606 nm, typically attributed to the $4f^65d^1 \rightarrow 4f^7$ electronic dipole allowed transitions of Eu^{2+} ions. The PL spectra showed a strong broad asymmetric yellow-emission in the wavelength range 450–800 nm, corresponding to the allowed $4f^65d^1 \rightarrow 4f^7$ electronic transitions of Eu^{2+} . The PL spectra of the $\text{SMGP}:0.01\text{Eu}^{2+}$ phosphor were deconvoluted into five Gaussian profiles with peaks centered at 506, 541, 591, 642, and 691 nm, which were ascribed to five different emission sites identified as the different coordination environments of the Eu^{2+} ions.^{21,24} The PLE spectrum showed a broad absorption band between 240 and 500 nm, attributed to the $4f^7 \rightarrow 4f^65d^1$ transition of the Eu^{2+} ions; this absorption band was well consistent with the reflectance spectra and NUV chips. These observations indicated that $\text{SMGP}:\text{xEu}^{2+}$ phosphors can be combined with NUV chips for white-light NUV LED applications.

Electroluminescence properties

White-light LED lamps were fabricated by integrating a mixture of transparent silicone resin and a phosphor blend comprising

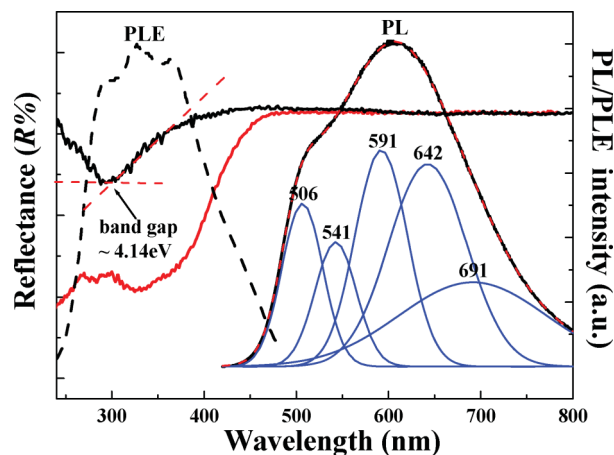


Fig. 4 Reflectance spectra of $\text{Sr}_8\text{MgGd}(\text{PO}_4)_7$ and $\text{Sr}_8\text{MgGd}(\text{PO}_4)_7:0.01\text{Eu}^{2+}$, and PL/PLE spectra of $\text{Sr}_8\text{MgGd}(\text{PO}_4)_7:0.01\text{Eu}^{2+}$ phosphor.

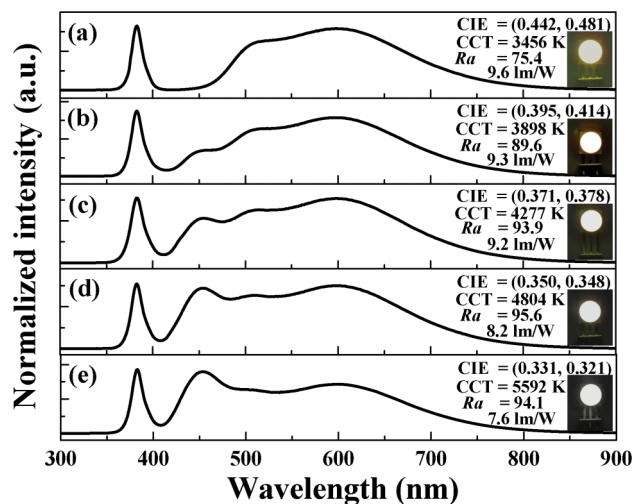


Fig. 5 EL spectra of white-light LEDs composed of a 385 nm NUV chip and a phosphor blend of blue-emitting $\text{BaMgAl}_{10}\text{O}_{17}:\text{Eu}^{2+}$ and yellow-emitting $\text{Sr}_8\text{MgGd}(\text{PO}_4)_7:0.01\text{Eu}^{2+}$ in various mixing ratios.

blue-emitting $\text{BaMgAl}_{10}\text{O}_{17}:\text{Eu}^{2+}$ (BAM: Eu^{2+}) and yellow-emitting $\text{SMGP}:0.01\text{Eu}^{2+}$ in various mixing ratios, on a commodity 385 nm NUV LED chip (AOT, Taiwan, Product No: DC0008CAA, Spec: 385V04C, wavelength peak: $380\text{--}385 \pm 0.94$ nm, chip size: 40×40 mil², forward voltage: $3.8\text{--}4.0 \pm 0.02$ V, power: $30\text{--}40 \pm 1.66$ mW), which was then annealed at 120°C for 10 h. The LEDs were driven at 350 mA. Fig. 5 shows the electroluminescence (EL) spectra of the lamps. Three emission bands can be clearly seen in Fig. 5a: 383 nm, attributed to the NUV chip; 512 and 606 nm, attributable to the SMGP: 0.01Eu^{2+} phosphor. Fig. 5b–e show four emission bands: 383, attributed to the NUV chip; 454 nm, attributed to BAM: Eu^{2+} ; and 512 and 606 nm, attributed to the SMGP: 0.01Eu^{2+} phosphor. Accordingly, the CCT and CRI could be tuned to convert yellow light (3456 K, 75.4, Fig. 5a) into warm white-light (4804 K, 93.9, Fig. 5d) and then to white-light (5592 K, 94.1, Fig. 5e). The CRI gradually increased with the BAM: Eu^{2+} phosphor mixed ratio, reaching a maximum at 95.6 (Fig. 5d), and then decreased with a further increase in the BAM: Eu^{2+} mixed ratio. The luminous efficacies of the fabricated white LEDs were measured to be 9.6, 9.3, 9.2, 8.2 and 7.6 lm W^{-1} for Fig. 5a to Fig. 5e. The lower values of luminous efficacy were due to poor chip efficiency ($30\text{--}40 \pm 1.66$ mW). The insets show photographs of the LED lamp packages driven by 350 mA current. The 14 CRIs and average CRI values of white-light LEDs driven by 350 mA current are listed in Table 2. The results indicate that the SMGP: 0.01Eu^{2+} /BAM: Eu^{2+} blends had suitable

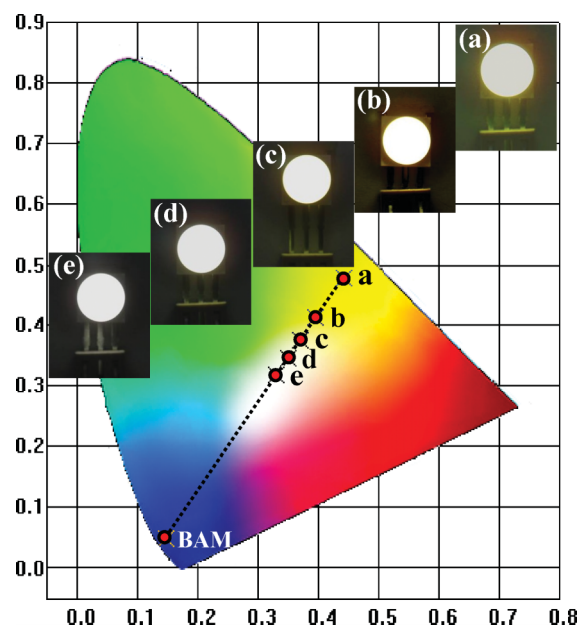


Fig. 6 CIE chromaticity diagram of white-light LEDs with $\text{BaMgAl}_{10}\text{O}_{17}:\text{Eu}^{2+}$ and $\text{Sr}_8\text{MgGd}(\text{PO}_4)_7:0.01\text{Eu}^{2+}$ in various mixing ratios. The insets show photographs of the LED packages driven by 350 mA current.

ble colors and that the CCT and CRI values were suitable for the application of these blends in white-light NUV LEDs.

Fig. 6 shows the CIE chromaticity diagram of white-light LEDs with various BAM: Eu^{2+} /SMGP: 0.01Eu^{2+} mixing ratios. By weight ratio tuning, the outputs of the BAM: Eu^{2+} and SMGP: 0.01Eu^{2+} phosphors were found to systematically emit hues and chromaticity coordinates (x , y) of white-light LEDs from yellow (point a, (0.442, 0.481)) through warm white-light (point c, (0.371, 0.378)) and eventually to the white-light (point e, (0.331, 0.321)) region with increasing BAM: Eu^{2+} weight ratio. The insets show photographs of the LED packages with a 385 nm NUV chip, driven by 350 mA current. For comparison, YAG: Ce^{3+} pumped with an InGaN blue chip was considered, and this system was found to emit white-light with chromaticity coordinates, CCT, and CRI of (0.292, 0.325), 7756 K, and 75, respectively.⁹ The white-light NUV LEDs fabricated in this study (point d) showed higher CRI values (95.6 for SMGP: 0.01Eu^{2+} , 75 for YAG: Ce^{3+}) and lower CCT values (4804 K for SMGP: 0.01Eu^{2+} , 7756 K for YAG: Ce^{3+}). The results obtained for the LED package demonstrated that SMGP: 0.01Eu^{2+} has potential applications in the white-light NUV LEDs with excellent CRIs.

Table 2 14 CRIs and average CRI values of white-light LEDs fabricated from blue-emitting $\text{BaMgAl}_{10}\text{O}_{17}:\text{Eu}^{2+}$ and yellow-emitting $\text{Sr}_8\text{MgGd}(\text{PO}_4)_7:0.01\text{Eu}^{2+}$ with a 385 nm NUV chip driven by 350 mA current

	R1	R2	R3	R4	R5	R6	R7	R8	R9	R10	R11	R12	R13	R14	CRI
a	81	82	79	63	78	81	72	67	27	67	59	68	80	91	75.4
b	88	93	96	88	88	93	92	79	45	86	88	82	89	98	89.6
c	93	98	97	93	94	98	93	85	62	96	94	89	95	98	93.9
d	98	98	96	96	97	95	94	91	80	96	98	90	99	98	95.6
e	93	93	97	95	92	90	95	98	94	86	92	86	91	98	94.1

Conclusions

A warm white-light LED device with an excellent CRI has been fabricated for the first time using a yellow-emitting phosphor $\text{Sr}_8\text{MgGd}(\text{PO}_4)_7:x\text{Eu}^{2+}$, and its luminescence properties, reflectance spectra, and electroluminescence performance have been investigated. Non-radiative transitions between the Eu^{2+} ions in the $\text{Sr}_8\text{MgGd}(\text{PO}_4)_7$ host are attributable to dipole–dipole interactions. The reflectance spectra show strong broad absorption in the 240–470 nm (NUV to blue) range, which matches well with those of NUV LED chips. The optical properties of the white-light LEDs (CRI = 95.6 at a CCT of 4804 K, with CIE coordinates of (0.350, 0.348)) are superior to those of conventional white-light LEDs based on YAG:Ce³⁺ pumped with blue LED chips (CIE = (0.292, 0.325), CRI = 75, CCT = 7756 K).⁹ Therefore, our novel yellow-emitting $\text{Sr}_8\text{MgGd}(\text{PO}_4)_7:x\text{Eu}^{2+}$ phosphor can serve as a key material for phosphor converted warm white-light NUV LEDs.

Acknowledgements

This research was supported by the Industrial Technology Research Institute under contract No. B352A31440 (Y. T. Y.) and No. B301AR4850 (C. H. H.) and in part by the National Science Council of Taiwan under contract No. NSC98-2113-M-009-005-MY3 (T. M. C.).

References

- 1 S. Nakamura, T. Mukai and M. Senoh, *Appl. Phys. Lett.*, 1994, **64**, 1687.
- 2 S. Ye, F. Xiao, Y. X. Pan, Y. Y. Ma and Q. Y. Zhang, *Mater. Sci. Eng., R*, 2010, **71**, 1.
- 3 W. B. Im, Y. I. Kim, N. N. Fellows, H. Masui, G. A. Hirata, S. P. DenBaars and R. Seshadri, *Appl. Phys. Lett.*, 2008, **93**, 091905.
- 4 T. Nishida, T. Ban and N. Kobayashi, *Appl. Phys. Lett.*, 2003, **82**, 3817.
- 5 S. Muthu, F. J. P. Schuurmans and M. D. Pashley, *IEEE J. Sel. Top. Quantum Electron.*, 2002, **8**, 333.
- 6 S. Lee and S. Y. Seo, *J. Electrochem. Soc.*, 2002, **149**, J85.
- 7 Z. Hao, J. Zhang, X. Zhang, X. Sun, Y. Luo, S. Lu and X. Wang, *Appl. Phys. Lett.*, 2007, **90**, 261113.
- 8 J. S. Kim, P. E. Jeon, Y. H. Park, J. C. Choi, H. L. Park, G. C. Kim and T. W. Kim, *Appl. Phys. Lett.*, 2004, **85**, 3696.
- 9 C. H. Huang and T. M. Chen, *Opt. Express*, 2010, **18**, 5089.
- 10 C. H. Huang, Y. C. Chen, T. W. Kuo and T. M. Chen, *J. Lumin.*, 2011, **131**, 1346.
- 11 C. Guo, L. Luan, Y. Xu, F. Gao and L. Liang, *J. Electrochem. Soc.*, 2008, **155**, J310.
- 12 T. G. Kim, Y. S. Kim and S. J. Im, *J. Electrochem. Soc.*, 2009, **156**, J203.
- 13 Y. C. Chiu, W. R. Liu, C. K. Chang, C. C. Liao, Y. T. Yeh, S. M. Jang and T. M. Chen, *J. Mater. Chem.*, 2010, **20**, 1755.
- 14 C. H. Huang, P. J. Wu, J. F. Lee and T. M. Chen, *J. Mater. Chem.*, 2011, **21**, 10489.
- 15 P. Thiyagarajan, M. Kottaisamy and M. S. Ramachandra Rao, *J. Phys. D: Appl. Phys.*, 2006, **39**, 2701.
- 16 Y. C. Chiu, C. H. Huang, T. J. Lee, W. R. Liu, Y. T. Yeh, S. M. Jang and R. S. Liu, *Opt. Express*, 2011, **19**, A331.
- 17 Z. Hao, J. Zhang, X. Zhang, X. Sun, Y. Luo, S. Lu and X. J. Wang, *Appl. Phys. Lett.*, 2007, **90**, 261113.
- 18 C. H. Huang and T. M. Chen, *J. Phys. Chem. C*, 2011, **115**, 2349.
- 19 ICSD file no. 59722.
- 20 V. A. Vysotsy, S. B. Gordon, H. L. Frisch and J. M. Hammersley, *Phys. Rev.*, 1961, **123**, 1566.
- 21 C. H. Huang and T. M. Chen, *Inorg. Chem.*, 2011, **50**, 5725.
- 22 D. L. Dexter, *J. Chem. Phys.*, 1953, **21**, 836.
- 23 L. G. Vanuiter, *J. Electrochem. Soc.*, 1967, **114**, 1048.
- 24 C. H. Huang, Y. C. Chen, T. M. Chen, T. S. Chan and H. S. Sheu, *J. Mater. Chem.*, 2011, **21**, 5645.
- 25 C. H. Huang, T. M. Chen, W. R. Liu, Y. C. Chiu, Y. T. Yeh and S. M. Jang, *ACS Appl. Mater. Interfaces*, 2010, **2**, 259.